Validation Against ASIRAS
SAMOSA2 WP2300

ESRIN Contract N. 20698/07/I-LG

Lars Stenseng and Christine Gommenginger
Technical Note. Version 1.1
January 28, 2011

DTU Space
National Space Institute

National Oceanography Centre
NATURAL ENVIRONMENT RESEARCH COUNCIL

Validation Against ASIRAS
SAMOSA2 WP2300.
ESRIN Contract N. 20698/07/I-LG

Lars Stenseng and Christine Gommenginger
National Space Institute
Technical Note. Version 1.1, Copenhagen, January 28, 2011

ISBN: 978-87-92477-07-1

http://www.space.dtu.dk

Contents

Document history

Version	Date	Affected sections	Comment
0.9	December 21, 2010		Initial draft
1.1	January 28, 2011	4.1, 4.3, 4.4, 5, and B	Response to ESA review

Table 1: Document history

1 Introduction

The aim of this document is to evaluate the performance of the SAR altimeter re-tracker against real data.

According to the project plan the work packet is divided into the following tasks:

- Apply beam selection technique developed in SAMOSA WP8 (Stenseng, 2009) to re-processed ASIRAS data. This procedure selects only beams with a look angle off less than 1.4,$^\circ$ as those with higher look angles were found to degrade the waveforms.
- Characterise the parameters to use in the NOCS SAR waveform re-tracker developed in SAMOSA WP5 (Gommenginger and Srokosz, 2009) to accommodate ASIRAS data. Provide ASIRAS data in format suitable for ingestion by the NOCS SAR retracker
- Apply the NOCS SAR waveform re-tracker to ASIRAS data.
- Produce Technical Note on the ASIRAS waveforms retracking for purpose of NOCS retracker validation.

2 Comparison of space- and airborne SAR altimeters

The differences between space- and airborne altimeters is mainly caused by the different geometry, but for SAR altimeters the platform velocity and hence the Doppler shift also play an important role. As a consequence of the geometry the footprint of a space-borne radar will be pulse limited whereas an air-borne radar often will be beam limited. Table 2 gives an overview of the main properties of the CryoSat-2 SIRAL instrument operating in SAR mode and ASIRAS operating in HAM.

To obtain a pulse repetition frequency (PRF) high enough to unambiguously sample the Doppler spectrum of the returned pulses CryoSat uses burst strategy. A burst of 64 pulses is emitted from the radar with the needed PRF, shortly after the last pulse has been emitted the first pulse arrives back at the radar after being reflected from the surface. After 11.7 ms[1] all 64 pulses has been received and the next burst is emitted.

The short round trip time associated with a low altitude airborne radar allows a pulse to travel from the radar to the surface and back before the next pulse is emitted. The round trip time combined with the pulse length dictates the upper limit on the PRF and the lower limit is limited by the Doppler spectrum that follows the along-track beam width and the platform velocity. All pulses are separated equally in time which allows the burst size for the airborne radar to be chosen during post processing.

Parameter	Description	CryoSat-2 SAR	ASIRAS HAM
λ	Carrier radar wavelength	0.022 m	0.022 m
f	Carrier radar frequency	13.575 GHz	13.5 GHz
h	Height above surface	717.242 km	2.738 km
α_R	Orbital factor	1.12	1.00
v	Velocity	7 km/s	70.5 m/s
f_{PRF}	Pulse repetition frequency	17.8 kHz	2.5 kHz
$\widehat{f_{PRF}}$	Average pulse repetition frequency	5.47 kHz	2.5 kHz
γ	Antenna 3 dB beam width (along-track)	1.0766°	10°
	Antenna 3 dB beam width (cross-track)	1.2016°	2.5°

Table 2: Properties for CryoSat-2 SAR mode and ASIRAS HAM.

Using the parameters presented in Table 2 and Equation 1 the along-track Doppler resolution can be calculated as a function of the burst size.

$$\Delta x_{az} = \frac{\lambda \cdot h \cdot f_{PRF}}{2 \cdot v \cdot N_{burst}} \tag{1}$$

ASIRAS has been build with a wide along-track beam to accommodate flight over steep terrain at a constant height over the surface. Also the pitch of the aircraft will change depending on the amount of cargo and general flying conditions.

With the high along-track look angle it is possible to get a high number of equivalent looks for the summation. However at a certain critical angle (θ_c) the width of the Doppler beam projected onto the pointing vector becomes comparable to the range resolution and will no longer benefit the resulting waveform. Over this critical angle (θ_c), see Equation 2, the Doppler beams will instead degrade the resulting waveform (Stenseng, 2009). The

[1]The 11.7 ms burst period is for the SAR mode only. SARin mode uses a burst period of 46.7 ms.

scaling factor (a) can be chosen slightly higher than unity to obtain more looks at the cost of a slightly higher degradation.

$$\theta_c < a \cdot \frac{\Delta_{res}}{\Delta x_{az}} \tag{2}$$

The average PRF ($\widehat{f_{PRF}}$) is introduced as the number of pulses within a burst divided by the burst-period. Using the chosen beam width (θ) and the average PRF the number of expected looks can be found.

$$N_{looks} = \frac{\theta \cdot h \cdot \widehat{f_{PRF}}}{v \cdot N_{burst}} \tag{3}$$

3 ASIRAS data and processing

On April 30 2006 ASIRAS HAM data were collected along a profile from Danmarkshavn in Greenland to Longyearbyen on Svalbard, see Figure 1. The data were acquired between 10:08:49 and 10:23:05 UTC and covered a profile from 77°57'02.38" N, 4°39'41.85" W to 78°05'29.21" N, 2°08'21.05" W. The flight was part of the CryoVEx 2006 campaign (Stenseng et al., 2007) and is one of the very few examples of ASIRAS data from the open ocean.

Figure 2 shows the attitude of the aircraft during the acquisition of the ASIRAS profile. The ASIRAS antenna is mounted looking 2° backwards resulting in an pitch of the antenna close to 1.6° forward looking. Due to heavy side-wind there is an average roll of $-0.9°$ and an average yaw of $-2.6°$.

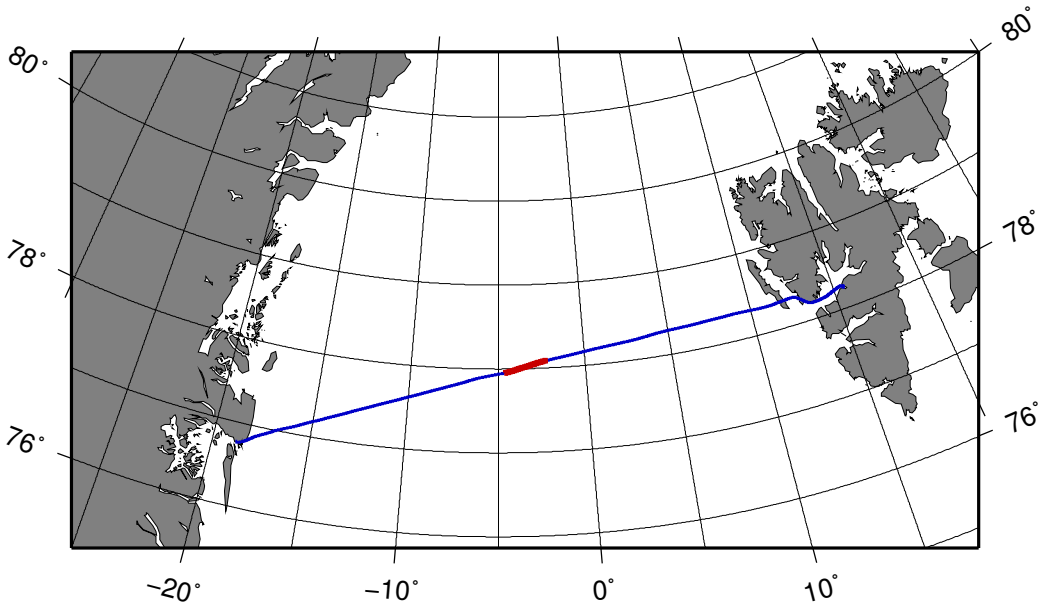

Figure 1: April 30 flight (blue) and profile where ASIRAS HAM data were collected (red), from Stenseng (2009).

3.1 ASIRAS processing

Since further correction and minor updates has been added to the ASIRAS processor and the default settings (Cullen, 2010), the profile has been reprocessed for this study using the final version of the processor (4.02) and the associated configuration files.

A series of processing scenarios has been run on the ASIRAS dataset varying the maximal look angle and the burst size. First the along-track size of the Doppler cell, the critical angle and the estimated number of looks is calculated based on the conditions for the ASIRAS data and a set of three different burst sizes, see Table 3.

Due to the high range resolution of ASIRAS the critical angle is quite small and as a result the number of equivalent look is reduced to 15. It is unlikely that the speckle noise will average out using only 15 look, therefore a slightly higher degradation factor (a in

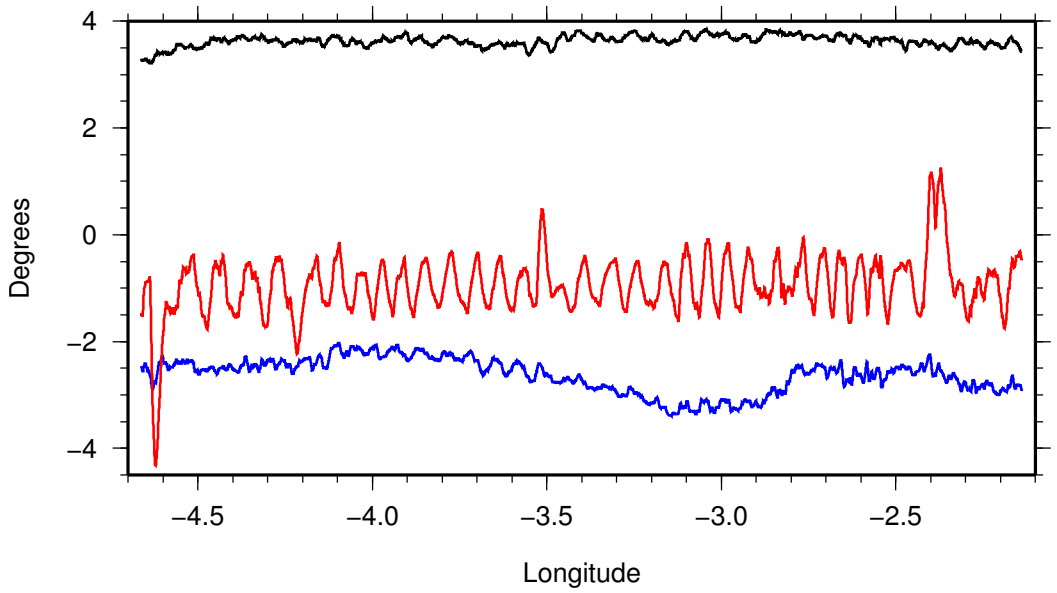

Figure 2: Attitude of the aircraft during acquisition of the ASIRAS profile. Roll in red, pitch in black and yaw in blue.

N_{burst}	Δx_{az}	θ_c	N_{looks}
64	16.69 m	0.30°	15
128	8.34 m	0.60°	15
256	4.17 m	1.2°	15

Table 3: Along track Doppler cell size, critical angle and number of looks as function of the burst size.

Equation 2) is used. A set of processor setting, including the standard, is prepared and used to generate four different scenarios from the single L0 ASIRAS profile. The discussed parameters is presented in Table 4.

Run	N_{burst}	Used max. look angle	Δx_{az}	N_{looks}
2001	128	6.0°	8.34 m	159
2002	128	1.4°	8.34 m	37
2012	64	1.4°	16.69 m	74
2022	256	1.4°	4.17 m	19

Table 4: Burst size and used look angle for the ASIRAS processing scenarios.

3.2 Along-track averaging

The high along-track resolution and the narrow cross-track beam width ($\sim$ 120 m) allows ASIRAS to sample small fractions of an ocean wave. From the profile in Figure 3 the minimum wave height can be estimated to 2 m, under the assumption that the vertical spread

in the the power arises from ASIRAS sampling the crest and the trough of the wave in separate samples. To obtain waveforms more representative of the ones CryoSat-2 observes, the ASIRAS L1b waveforms is averaged along-track.

For each processing scenario an along-track averaging of 10 and 20 waveforms has been performed. In Figure 4 the effect of the averaging the 2012 run is presented. The L1b waveforms without along-track averaging (Figure 4a) is very noisy and several of the individual waveforms are multi-peaked. The Effect of 10 and 20 waveforms along-track averaging is seen in Figure 4b and 4c. It is clear that the noise and double peaks is removed after a factor 10 averaging and further averaging only contributes to a more uniform power distribution in the range direction.

A closer inspection of the individual waveforms reveals almost symmetrical waveforms with a rapid decaying tail. This is most likely a consequence of the radar being beam-limited and having a relatively narrow cross-track beam width.

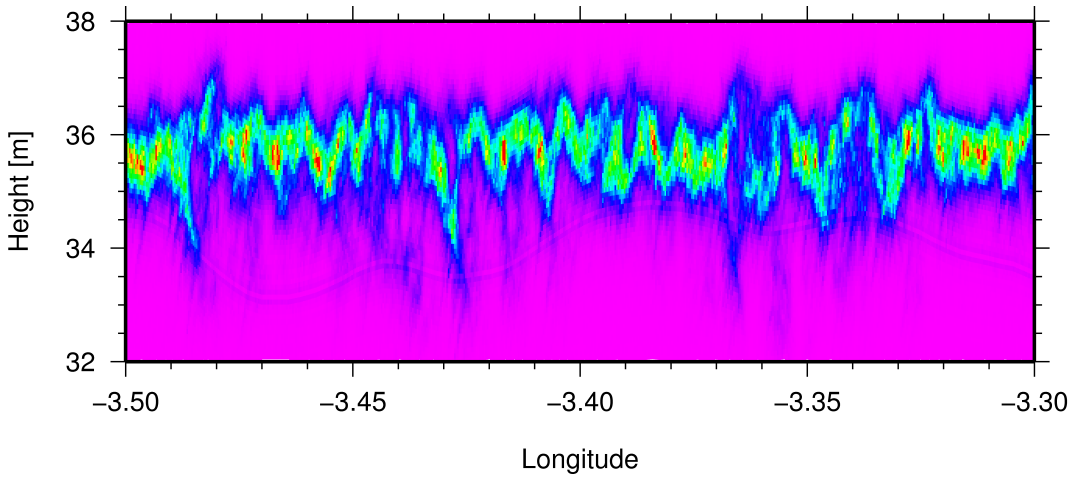

Figure 3: Part of the ASIRAS profile (run 2002) showing the power as function of the longitude and ellipsoidal height.

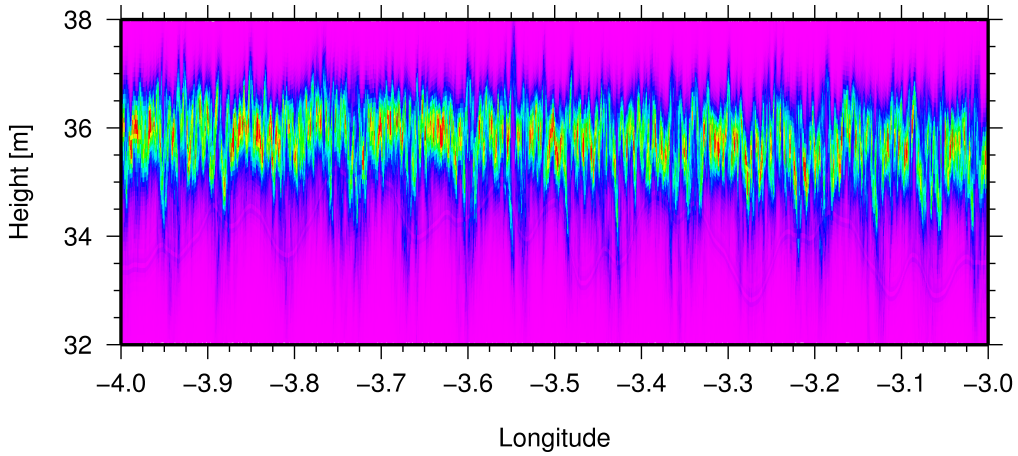

(a) L1b power waveforms from the 2012 scenario without along-track averaging.

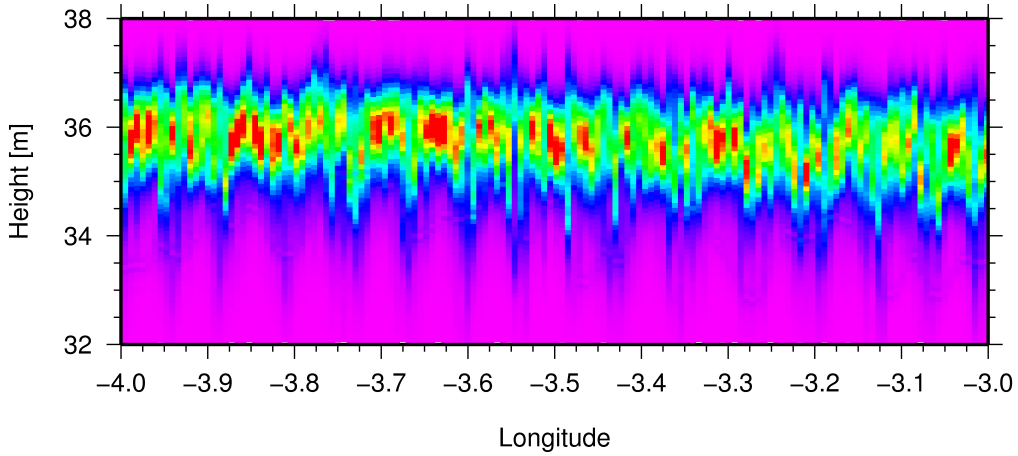

(b) L1b power waveforms from the 2012 scenario with a factor 10 along-track averaging.

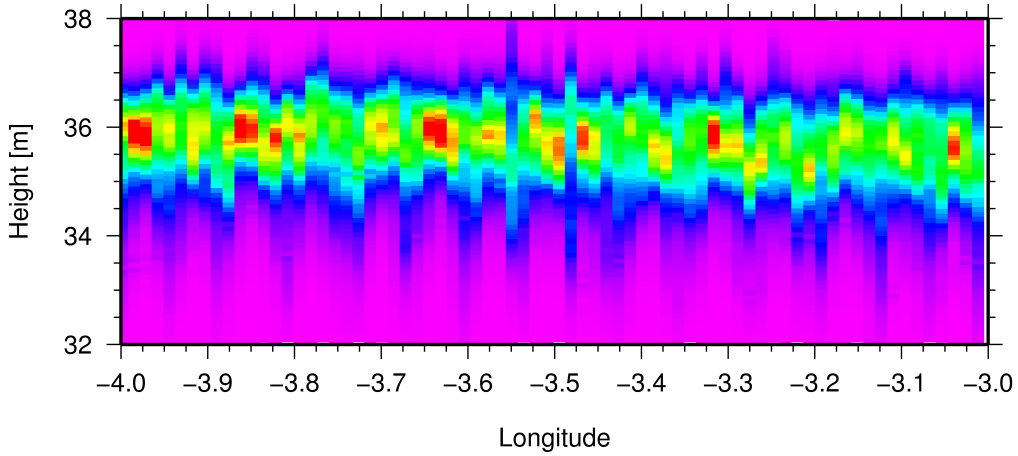

(c) L1b power waveforms from the 2012 scenario with a factor 20 along-track averaging.

Figure 4: Effect of along-track averaging on the 2012 scenario.

4 Retracking ASIRAS waveforms with the SAMOSA1 SAR retracker

The SAMOSA1 SAR retracker was developed in WP5 of the SAMOSA1 contract and WP4000 of the SAMOSA2 Contract Change Note to retrack SAR mode waveforms from spaceborne SAR altimeters over ocean surfaces. The retracker has been tested so far with SAR data obtained from CRYMPS scenarios over the open ocean and a small set of Cryosat-2 SAR waveform data over water (Gommenginger et al., 2010).

4.1 Adapting the SAMOSA1 SAR retracker to an airborne scenario

In this task, the SAMOSA1 retracker is adapted to retrack SAR waveforms from airborne flights of the ASIRAS system. The parameters used to run the retracker in an airborne configuration are given in Table 5, compared to the values used for the Cryosat-2 and CRYMPS configuration. The PTR Gaussian approximation coefficient is not know for ASIRAS and is therefore given the same value as for CryoSat-2.

	CRYMPS	CryoSat-2	ASIRAS
Transmitted bandwidth	320 MHz	320 MHz	1000 MHz
Gate spacing	3.125e-9 s	3.125e-9 s	0.585e-9 s
Number of gates	128	128	256
PRF	17.8e3 Hz	17.8e3 Hz	2.5e3 Hz
Number of echoes in burst Na	64	64	64, 128 or 256
Antenna 3dB along-track beamwidth Φ_B	1.3°	1.0766°	10.0°
Burst Repetition Interval	11.7e-3 s	11.7e-3 s	2.56e-2 s, 5.12e-2 s or 1.024e-1 s
Antenna max gain	42 dB	42 dB	26 dB
Pulse length	51e-6 s	51e-6 s	4e-6 s
PTR Gaussian approximation coeff. α_P	0.9	0.366	0.366
Mean platform velocity	7000 m/s	7000 m/s	70.5 m/s
Mean platform altitude	717242 m	717242 m	2774 m

Table 5: Parameter values used in SAMOSA1 SAR ocean retracker

We note that the retracker remains based on the same theoretical model and multi-looking approach as developed in SAMOSA1 for specific spaceborne systems. No adjustments were made for fundamental differences between the systems, such as:

- Different structure of the ASIRAS SAR signals from the CRYMPS and Cryosat-2 SAR Burst mode. Instead of a sequence of bursts of high PRF, ASIRAS emits pulses continuously at a constant PRF. The PRF around 2500Hz is considerably lower than for CRYMPS and Cryosat-2, and is only slightly higher than the PRF used by the Envisat RA-2 pulse-limited altimeter.

- Strongly asymmetric antenna beam width, with ASIRAS featuring a broad beam (10°) along-track and a relatively narrow beam (2.5°) across-track. The SAMOSA1 retracker is based on a theoretical model that assumes symmetric narrow beam.

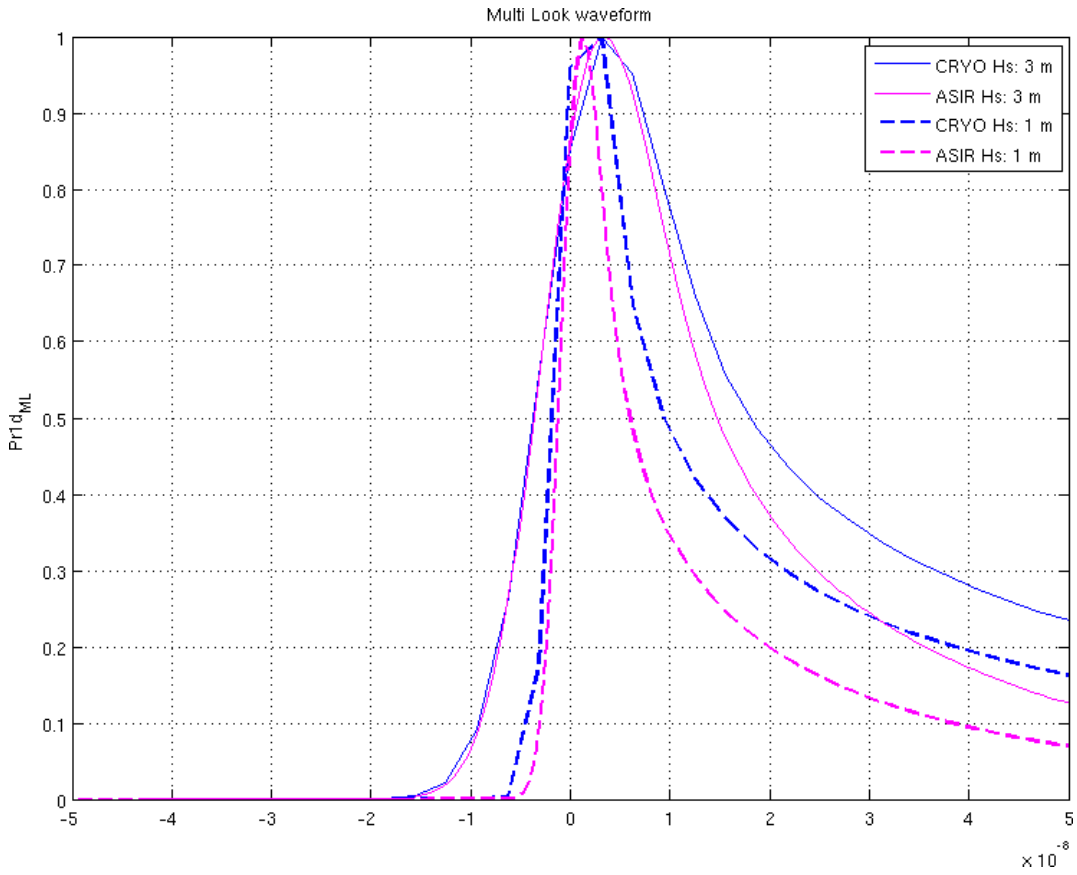

Figure 5: Simulated Multi-looked L1b waveforms with the SAMOSA1 SAR retracker model for satellite (Cryosat-2; Blue) and airborne (ASIRAS; Purple) configuration and two different sea state conditions (solid: Hs = 3m; dashed: Hs = 1m)

- Much smaller footprint for ASIRAS than in the case of space borne configurations, leading to different spatial and temporal correlations than in the case of a uniform rough surface (as assumed in the SAMOSA1 model).

Figure 5 compares the simulated L1b multi-looked SAR waveforms obtained in the airborne configuration to those in a Cryosat-2 configuration for two different significant wave height conditions. Both sets of waveforms are normalised. We note that according to the SAMOSA1 model, the airborne ASIRAS waveforms are expected to be much peakier than the spaceborne Cryosat-2 waveforms.

4.2 ASIRAS airborne HAM data

In this section, we examine the characteristics of the flight and ASIRAS waveforms prior to retracking. Figure 6 and Figure 7 show side and top views of the L1b SAR multi-looked waveforms as the aircraft travels along its track. The position of the waveforms along-track is indicated by longitude (vertical axis in Figure 7). The four subplots correspond to the data obtained for the same flight but four different processing choices, as described in the

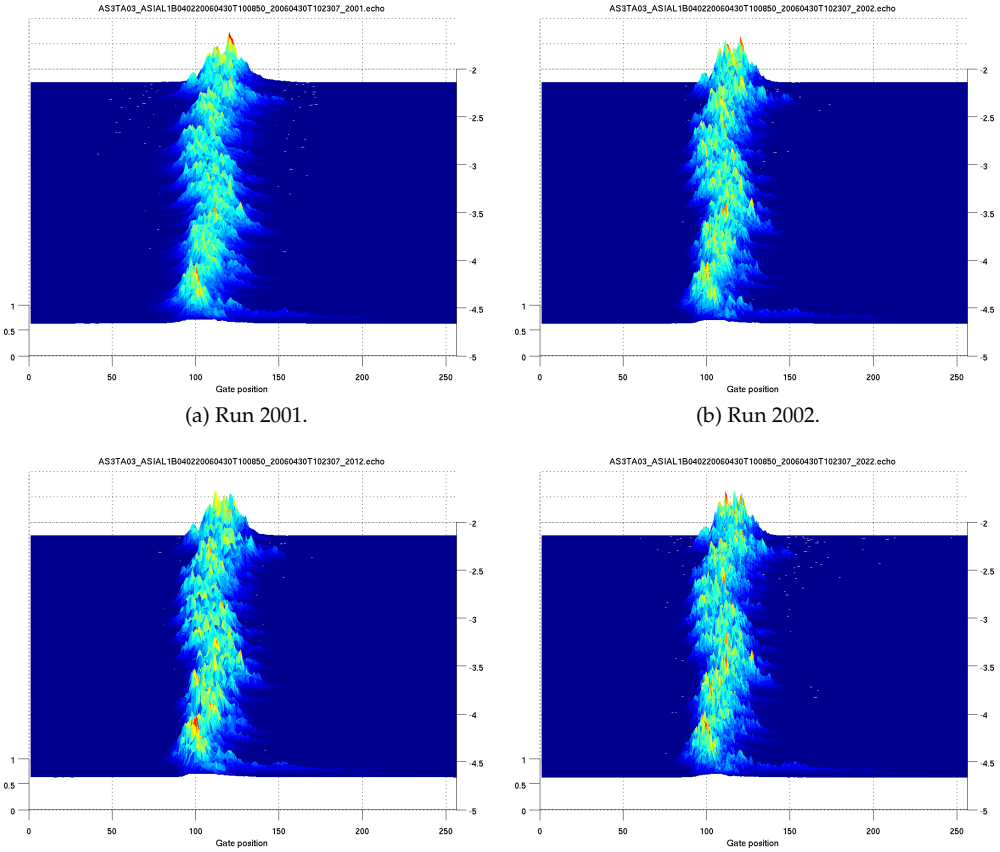

(a) Run 2001.

(b) Run 2002.

(c) Run 2012.

(d) Run 2022.

Figure 6: ASIRAS L1b SAR waveforms for the same airborne flight and different processing runs. The averaging characteristics for each run are shown in Table 4. All waveforms were scaled to the maximum amplitude in the run.

previous section. Figure 8 shows a zoomed-in section from Figure 7.

Examples of individual L1b waveforms at various positions along the track and for the different processing choices are shown in Section 4.4

Several observations can be made about the ASIRAS data from these figures:

- Limiting the Doppler beam angles in the processing leads to peakier waveforms, seen both as a slight reduction in the width of the waveforms (Figure 6) and an increase in the peak magnitude (Figure 7).
- There is considerable variability in the position of the leading edge along the flight track (Figure 6, Figure 7), including short episodes when the signals almost vanish (Figure 8).
- As well as the low-frequency variability in range, associated with the height and attitude of the aircraft, we note also some higher frequency wave-like variability. Given the small footprint of the ASIRAS system, it is possible that the altimeter was able to

sense the profile of individual ocean surface waves.

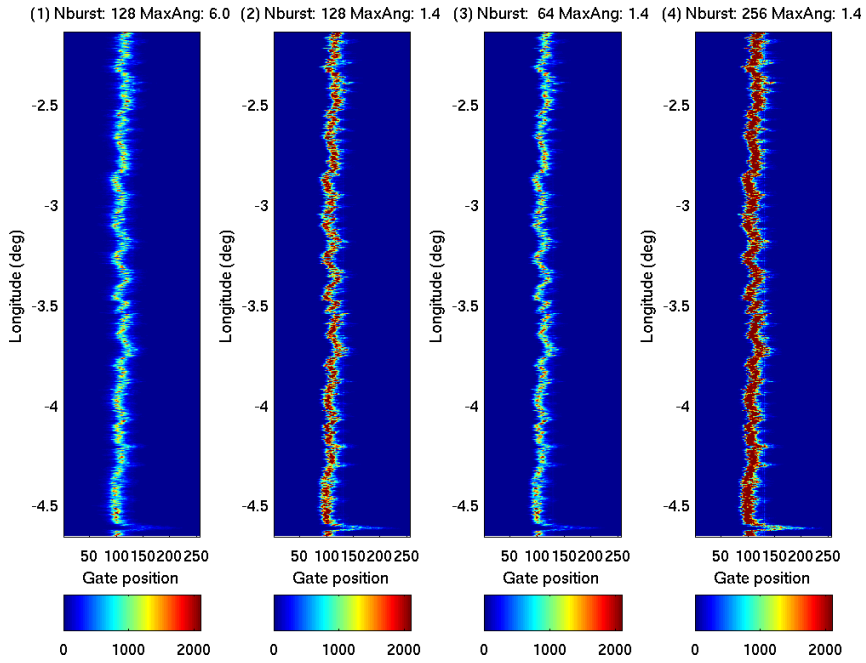

Figure 7: Same as Figure 6 but viewed from above showing ASIRAS L1b waveforms for (from left to right) run 2001, run 2002, run 2012, and run 2022. The waveform amplitudes were not scaled.

Figure 9 presents the evolution of the aircraft height and attitude along the track, together with the retracked range retrieved from an OCOG retracker (provided by DTU with the ASIRAS data). All data are plotted against longitude (on the vertical axis) and on the same scale for ease of comparison. We note:

- the strong correspondence between aircraft height and OCOG retrieved range.
- The reasonably steady (± 1 m) aircraft altitude, around 2774 meters.
- The large systematic pitch (i.e. along-track mispointing) averaging around 3.6° not including the 2° backwards pointing, with rapid sharp changes of the order of $\pm 0.2^\circ$ degrees in magnitude.
- The oscillating nature of the roll, averaging around -0.9° $\pm 0.5^\circ$.

The existence of large pitch and roll values are significant for the SAR retracking since:

- Pitch (i.e. along-track mispointing) is expected to strongly affect the positioning of the SAR waveforms (as well as the waveform shape).
- The magnitude of the roll (i.e. across-track mispointing) is significant in view of the narrow across-track beamwidth of the ASIRAS antenna. The large roll events may explain the signal drop-outs observed in the waveforms.

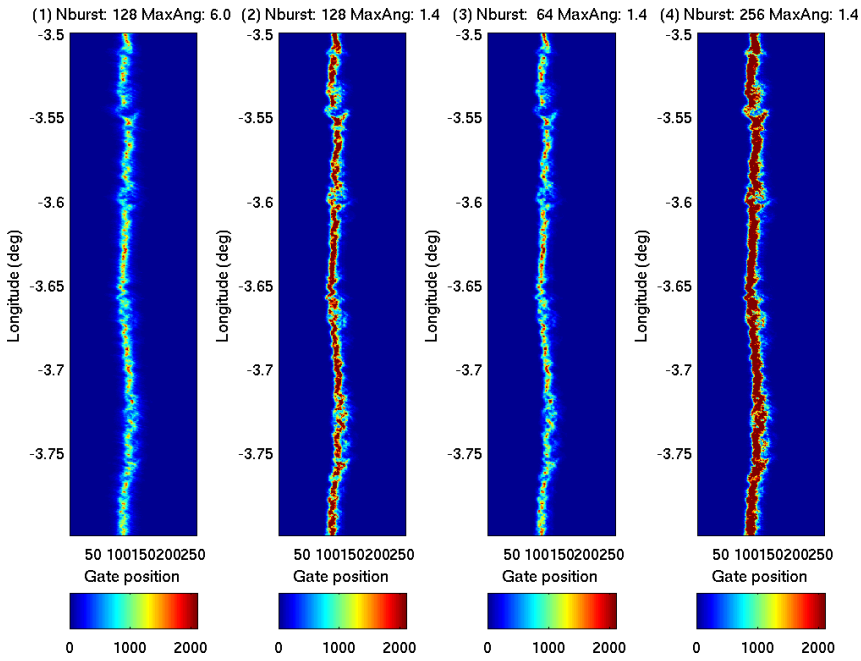

Figure 8: Zoomed-in section from Figure 7.

4.3 Along-track mispointing in the SAMOSA1 retracker

In this section, we examine the sensitivity of the SAMOSA1 retracker to along-track mispointing prior to retracking ASIRAS data. We note that the theoretical model on which the SAMOSA1 retracker only considers along-track mispointing.

We start by looking in Figure 10 at the waveforms simulated with the SAMOSA1 retracker in the case of zero (blue) and non-zero (green) mispointing for the ASIRAS (left) and Cryosat-2 (right) configuration. The top, middle and bottom subplots correspond to the single-look waveforms at zero Doppler frequency, the L1b multi-looked waveform (used by the retracker to fit the data) and the 2D Stack at zero Doppler frequency. In these plots, all waveforms were normalised by the maximum value at the peak. Based on these, one could conclude that there is no effect of mispointing on the shape of the waveforms.

Figure 11 now shows the same waveforms but without normalisation. It is immediately obvious that the 0.5 degrees of mispointing used here has a strong impact on the magnitude of the echo power in the case of CryoSat-2. Unlike expected the ASIRAS echo power is much less affected by the mispointing, this is due to the wide along-track beamwidth.

Figure 12 and Figure 13 show this effect in the multi-look 2D Stack prior to incoherent summing. Here, the stacks are shown plotted against Doppler Beam angles rather than Doppler frequency, and the range of these angles can be seen to span the whole width of the antenna beam. The main effect of the mispointing is to displace the peak power in the Stack in Doppler space.

We see from these figures that the effect of mispointing will be much more dramatic for space borne systems (Figure 12) than for airborne systems (Figure 13), for which the waveforms are not expected to be strongly affected. Accordingly, the retracking of ASIRAS

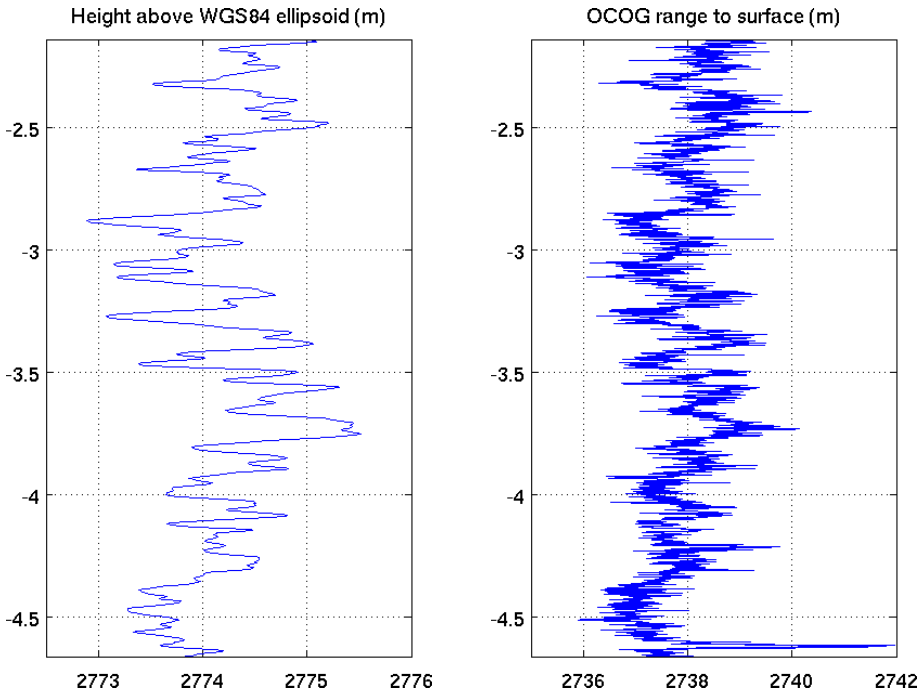

(a) Aircraft height above WGS84 ellipsoid.

(b) OCOG retracker range.

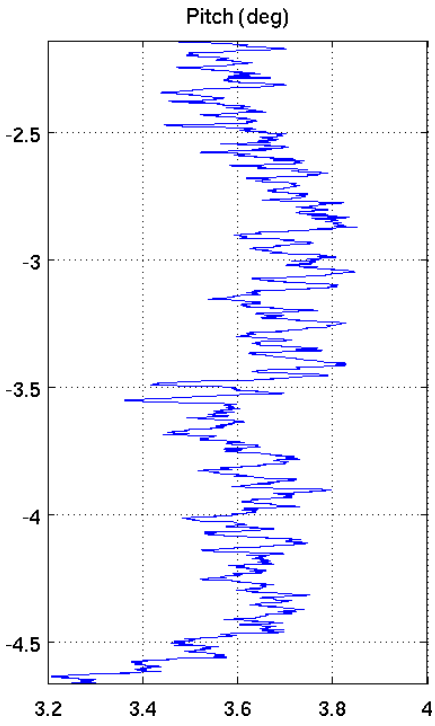

(c) Aircraft Pitch (i.e. along-track mispointing).

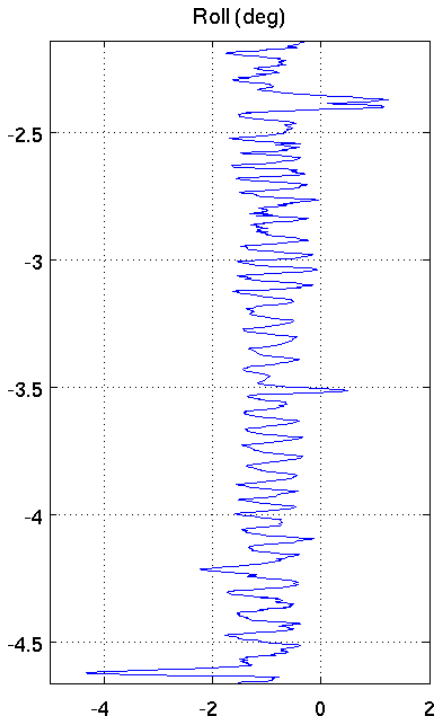

(d) Aircraft roll (i.e. across-track mispointing).

Figure 9: Aircraft height and attitude during the ASIRAS flight.

data will not account for along-track mispointing.

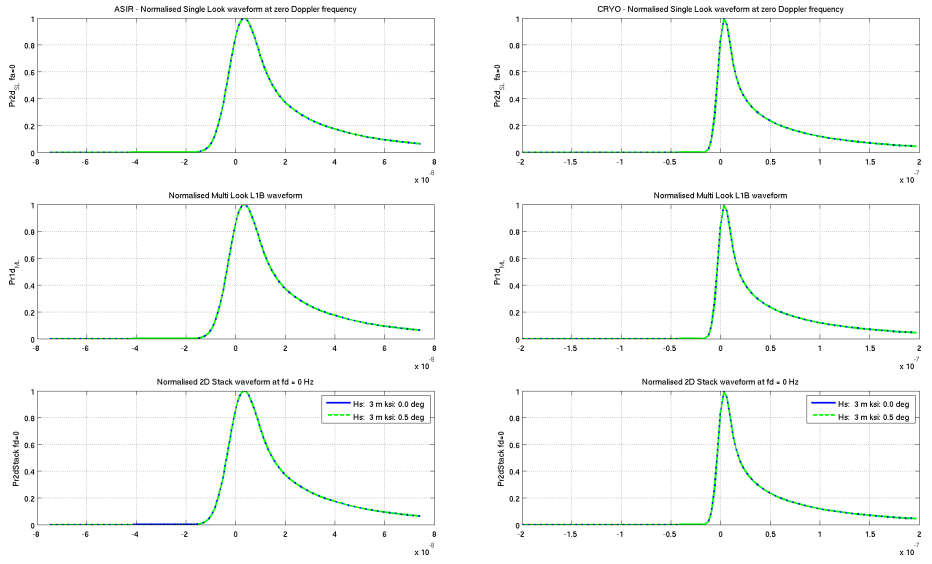

(a) (b)

Figure 10: Simulated SAR waveforms for (a) ASIRAS and (b) Cryosat-2 for along-track mispointing = 0 deg (blue) and 0.5 deg (green). The value of Hs is 3m in all cases. All waveforms are normalised by their maximum value.

4.4 Retracking ASIRAS L1b waveforms

We now apply the SAMOSA1 SAR retracker to the ASIRAS waveforms. To judge the appropriateness of the retracking, we examine a number of individual L1b waveforms at four different positions along the flight track. The locations were chosen at random and are indicated in Figure 14.

Figure 15 to Figure 18 represent the ASIRAS L1b waveform and the fitted model for the four different processing schemes, namely run 2001, 2002, 2012 and 2022. The estimated epoch and significant wave height are indicated in the legend on each plot, as well as the status of the fitting exitflag (a value of exitflag = 3 indicates that the optimisation was successful).

We note that in all cases, the best SAMOSA1 fitted model is unable to reproduce the rapidly decaying trailing edge of the ASIRAS waveforms, although ASIRAS seems to show stronger trailing edge in the latter part of the flight (Position 12, subplot d).

As noted previously, the ASIRAS waveforms are narrower in run 2002, 2012 and 2022, the modified processing being able to reduce the power at the toe of the leading edge. Consequently, the SAMOSA1 retracker is better able to fit the waveforms in run 2002, 2012 and 2022.

The surface height and significant wave height for all waveforms in Run 2001 are shown in Figure 19. The average surface height is found to be 36.24 m and the standard deviation 0.365 m when excluding the high roll events, only including points between 4.5° W and 2.5°

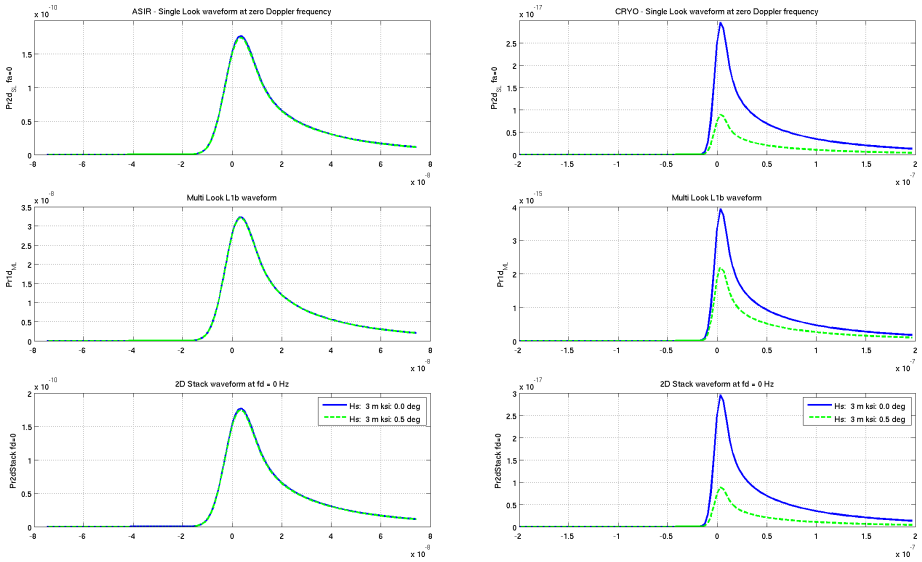

(a) (b)

Figure 11: Simulated SAR waveforms for (a) ASIRAS and (b) Cryosat-2 for along-track mispointing = 0 deg (blue) and 0.5 deg (green). The value of Hs is 3m in all cases. The waveforms in these plots are not normalised.

W. Repeating the calculating in a 100 measurement window gives a mean surface height between 35.71 m and 36.71 m and a standard deviation between 0.122 m and 0.589 m.

Adding the ASIRAS instrument correction found to be 3.487 m gives an true surface height of 39.72 m, which compares well with the 40.71 m estimated with the DTU10 Mean Sea Surface. It should be noted that the obtain surface height has not been applied tide or barometric corrections.

Repeating the calculations for the significant wave height gives an average of 1.26 m and a standard deviation of 0.529 m, again excluding points outside 4.5° W and 2.5° W. Using the 100 measurements window gives a mean between 0.89 m and 1.84 m with a standard deviation between 0.226 m and 0.772 m. We note again that the SAMOSA1 retracker seems unable to retrieve values of Hs below about 0.5 meters.

From the ECMWF wave model[2] the significant wave height is predicted to be 1.83 m at 06:00 UTC and 1.46 m at 12:00 UTC, which compares well with the significant wave height determined by the retracker.

From sea-ice data roll events are known to spread the echoes therefore a comparison between roll and significant wave height is carried out. Indeed Figure 20 shows a high correlation between roll and significant wave height. A similar investigation of the effect of pitch showed no significant correlation.

[2]Courtesy of Dr. Saleh Abdalla

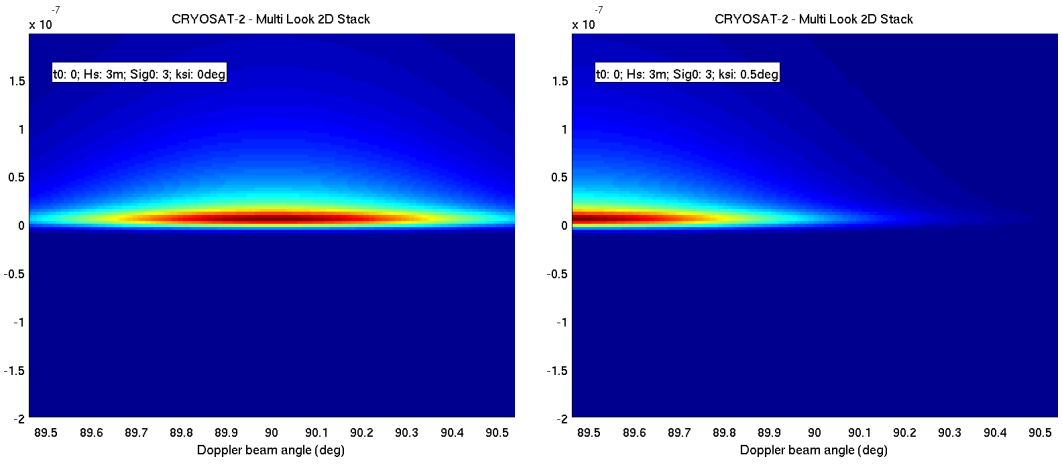

(a) (b)

Figure 12: Simulated single-look Delay Doppler Maps for CryoSat-2 configuration for a) along-track mispointing = 0 deg, b) along-track mispointing = 0.5 deg. The value of Hs is 3m in both cases.

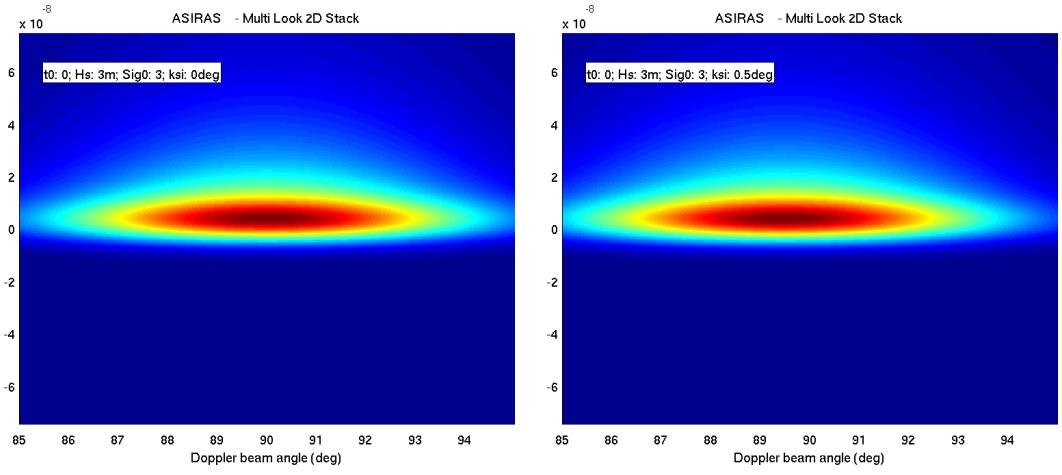

(a) (b)

Figure 13: Simulated single-look Delay Doppler Maps for ASIRAS configuration for a) along-track mispointing = 0 deg, b) along-track mispointing = 0.5 deg. The value of Hs is 3m in both cases.

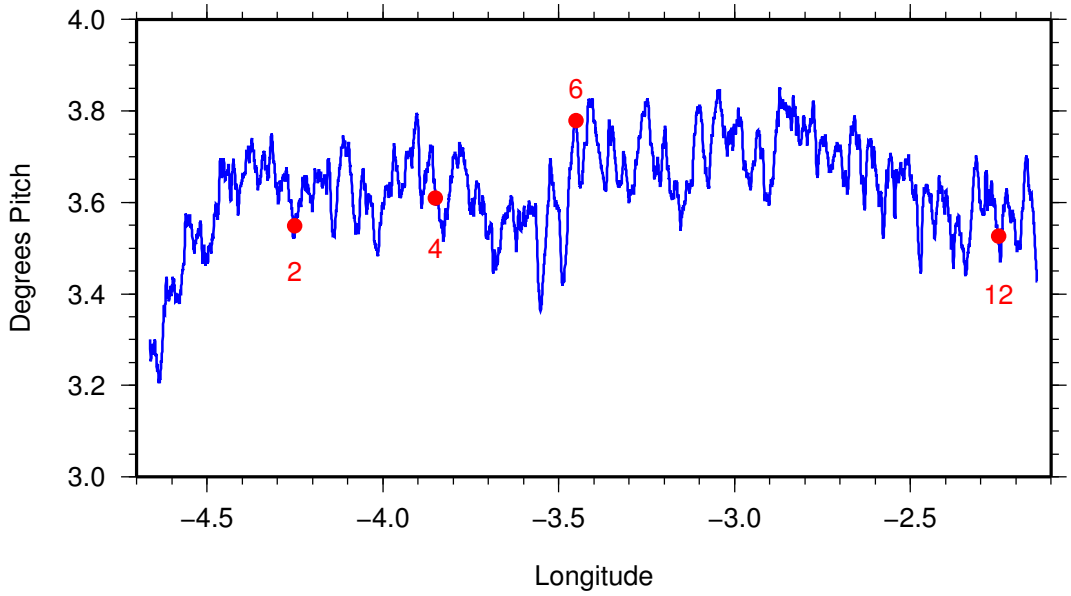

(a) Aircraft pitch during flight.

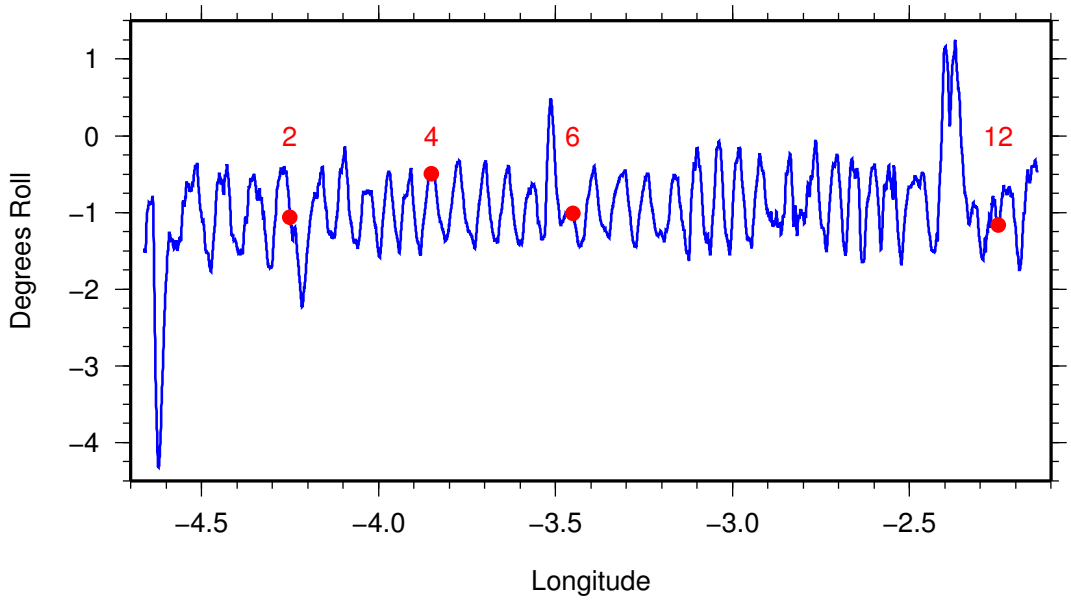

(b) Aircraft roll during flight.

Figure 14: Aircraft pitch during ASIRAS flight, showing the positions along-track of the waveforms shown in the figures below.

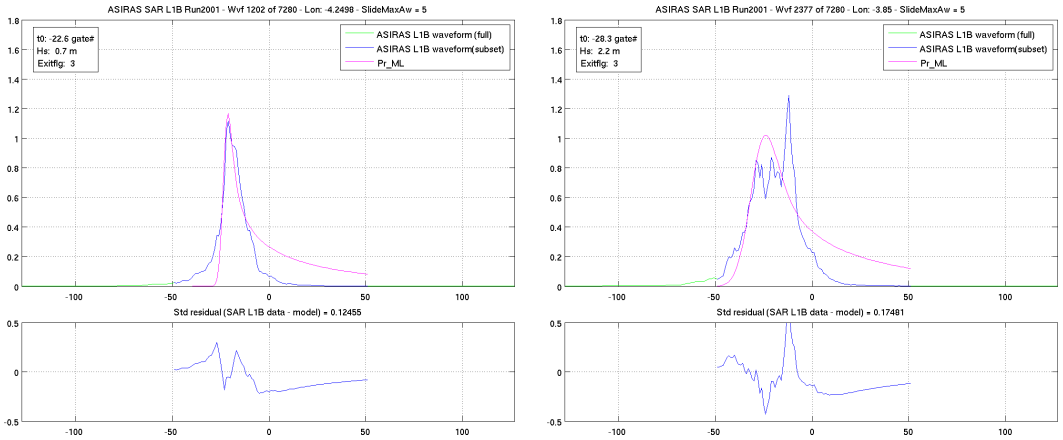

(a) Waveform position 2.

(b) Waveform position 4.

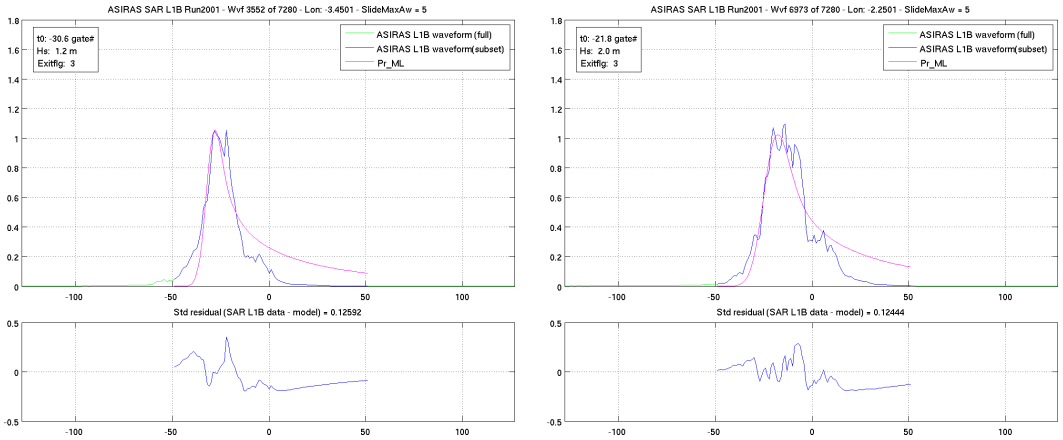

(c) Waveform position 6.

(d) Waveform position 12.

Figure 15: ASIRAS L1b SAR waveforms and fitted SAMOSA1 SAR waveform model for run 2001.

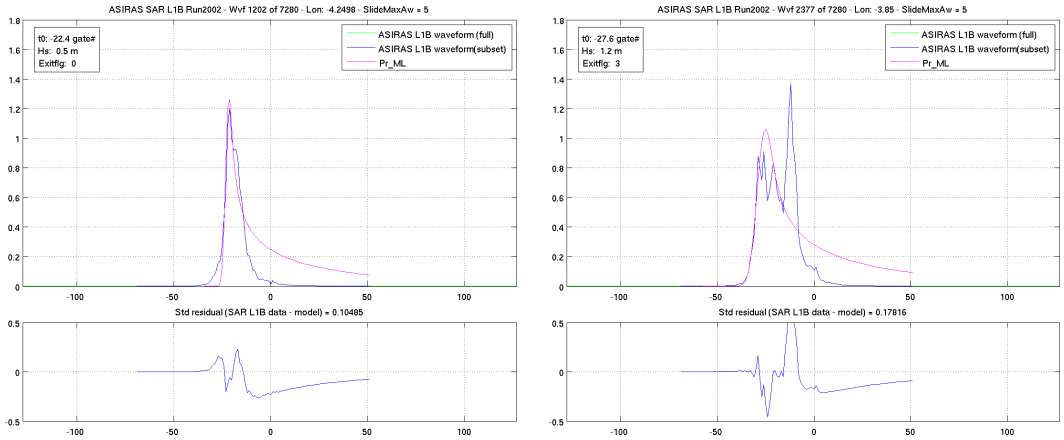

(a) Waveform position 2.

(b) Waveform position 4.

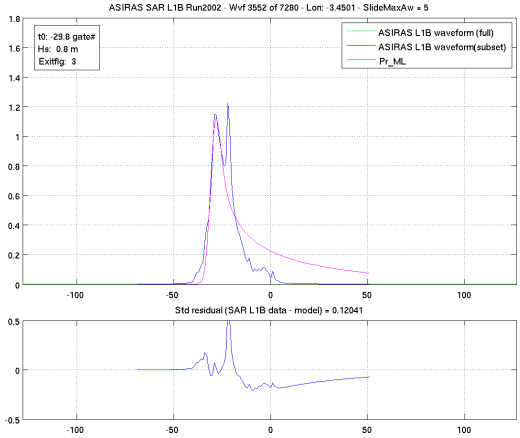

(c) Waveform position 6.

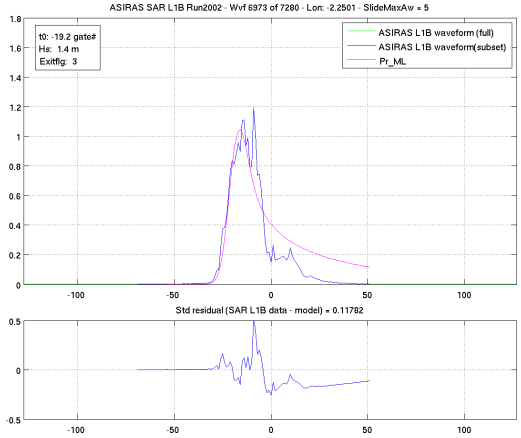

(d) Waveform position 12.

Figure 16: ASIRAS L1b SAR waveforms and fitted SAMOSA1 SAR waveform model for run 2002.

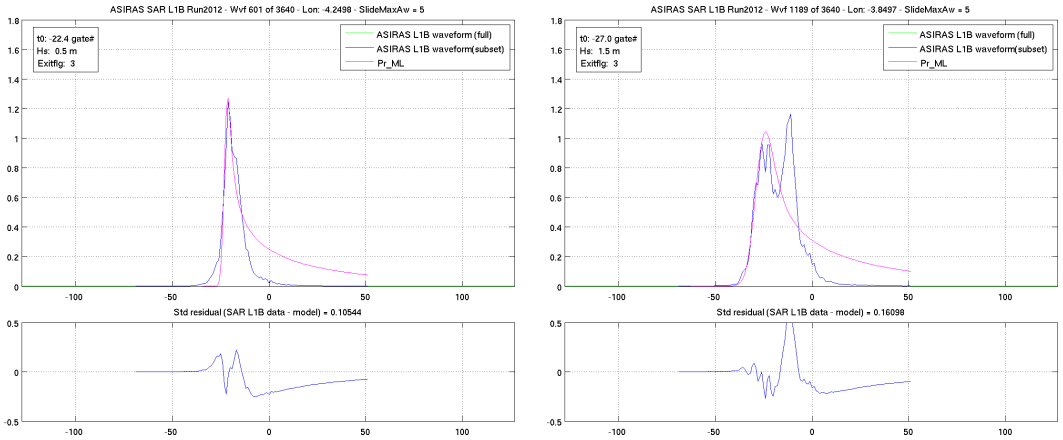

(a) Waveform position 2.

(b) Waveform position 4.

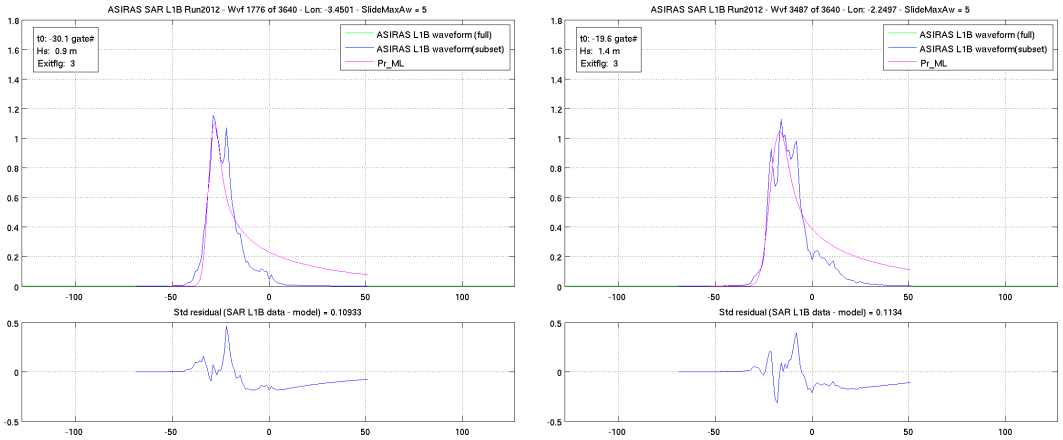

(c) Waveform position 6.

(d) Waveform position 12.

Figure 17: ASIRAS L1b SAR waveforms and fitted SAMOSA1 SAR waveform model for run 2012.

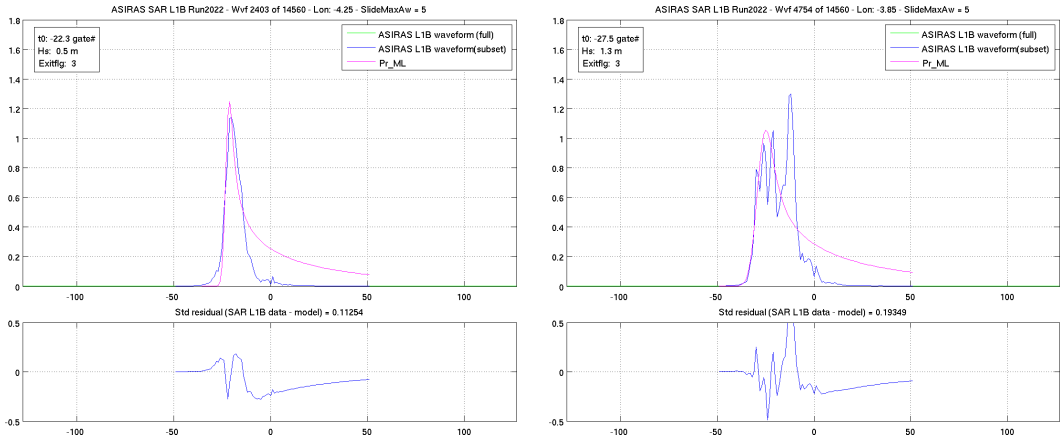

(a) Waveform position 2.

(b) Waveform position 4.

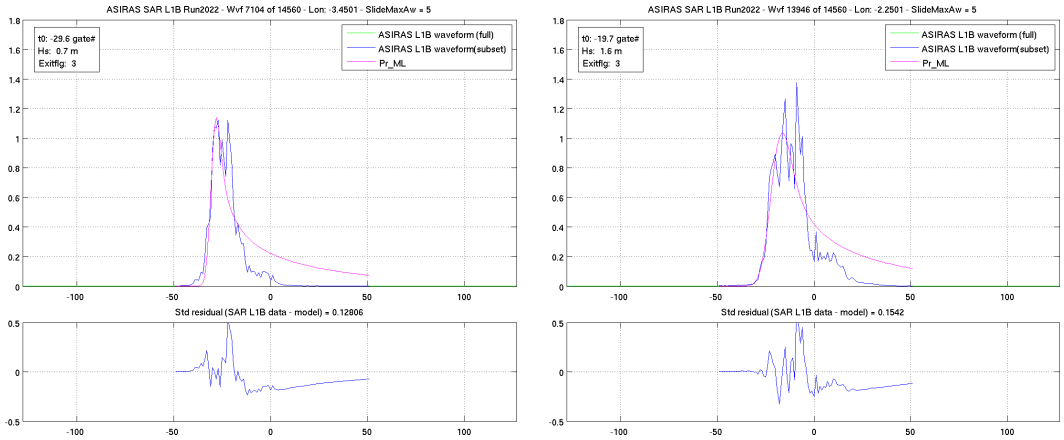

(c) Waveform position 6.

(d) Waveform position 12.

Figure 18: ASIRAS L1b SAR waveforms and fitted SAMOSA1 SAR waveform model for run 2022.

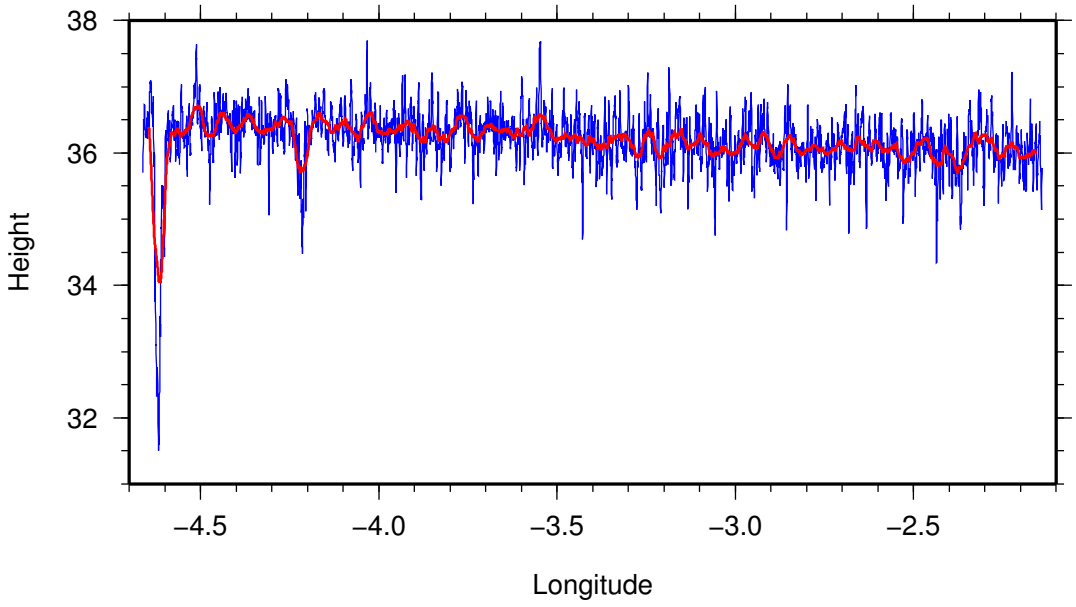

(a) Surface height.

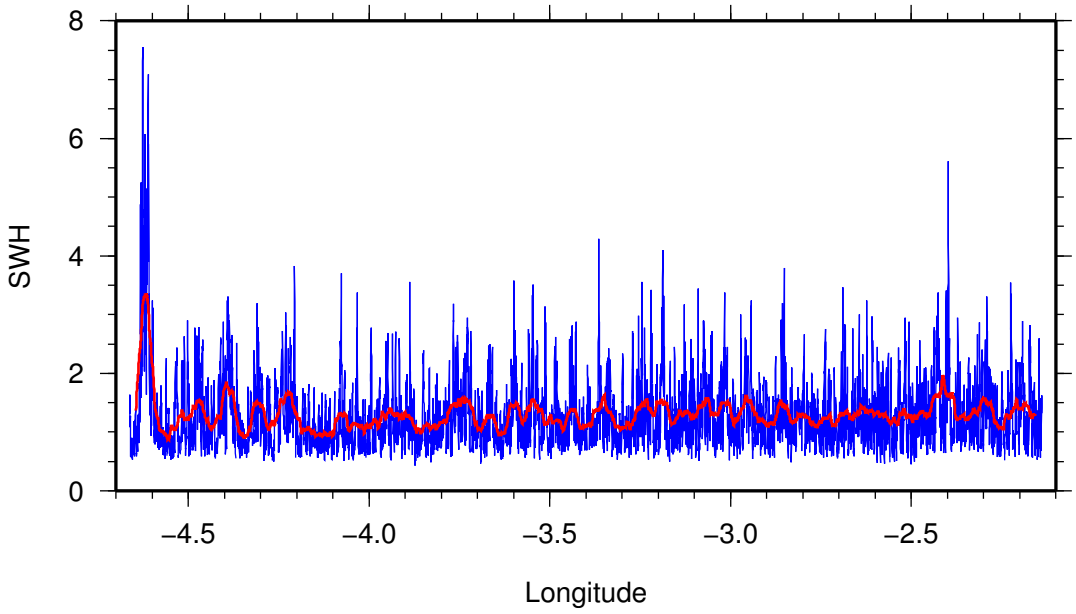

(b) Significant wave height.

Figure 19: Surface height (blue) and significant wave height (blue) with the SAMOSA1 SAR retracker for ASIRAS Run 2001. The results is overlayed with a 100 measurements running average.

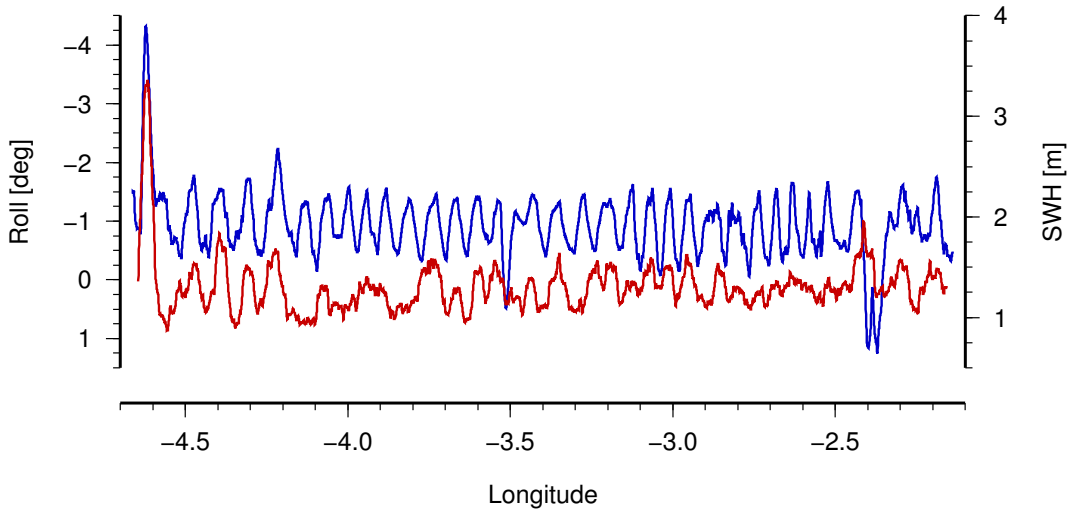

Figure 20: Aircraft roll (blue) and smoothed significant wave height (blue) for the SAMOSA1 SAR retracker for ASIRAS Run 2001.

5 Conclusion

The ASIRAS profile obtained in HAM over open ocean has been processed using four different processor settings. The different processing runs aimed at providing an optimal processing in the sense of providing a waveform closely reassembling a waveform obtained from a space-borne SAR altimeter, but scaled to airborne conditions.

The SAMOSA1 retracker has been applied on the four runs and waveforms at four randomly chosen positions has been investigated, see Figure 15 to 18. The main output parameters from the SAMOSA1 processor for all combinations of runs and positions is presented in Table 6.

From the figures and the table the following is noted:

- Run 2001 estimates a higher surface and significant wave height.
- Run 2002, 2012 and 2022 generally agree well on the estimated parameters.
- Except for a toe there is good agreement between the leading edge in ASIRAS data and model fitted by the SAMOSA1 retracker.
- The rapid decaying trailing edge in ASIRAS data is not captured by the SAMOSA1 retracker.
- Run 2012 has the best overall agreement with the fitted SAMOSA1 SAR waveform model.

Position / Run	2001	2002	2012	2022
2	-22.6 gate# 0.7 m 0.125	-22.4 gate# 0.5 m 0.105	-22.3 gate# 0.5 m 0.105	-22.3 gate# 0.5 m 0.113
4	-28.3 gate# 2.2 m 0.175	-27.6 gate# 1.2 m 0.178	-27.0 gate# 1.5 m 0.161	-27.5 gate# 1.3 m 0.193
6	-30.6 gate# 1.2 m 0.126	-29.8 gate# 0.8 m 0.120	-30.1 gate# 0.9 m 0.109	-29.6 gate# 0.7 m 0.128
12	-21.8 gate# 2.0 m 0.125	-19.2 gate# 1.4 m 0.118	-19.6 gate# 1.4 m 0.113	-19.7 gate# 1.6 m 0.154

Table 6: Leading edge position, significant wave height and std. residual output from the SAMOSA1 retracker.

The higher surface and significant wave height found in run 2001 is most likely due to the degradation associated with the high maximal look angle. The rapid decaying trailing edge is believed to be related to the narrow cross-track and along-track footprint not capturing an entire wave. The larger along-track Doopler bin in run 2012 is compensating for the short along-track footprint and a better agreement between the ASIRAS data and the SAMOSA1 waveform model is found.

The surface height and significant wave height estimated by the retracker is found to compare well with values obtained from the ECMWF wave model and the DTU10 Mean

Sea Surface. In overall the SAMOSA1 retracker is found to perform well with ASIRAS data when choosing an appropriate processing and tacking the fundamental differences between air- and space-borne systems into account.

References

Cullen, R. (2010). *CryoVEx Airborne Data Product Description*. European Space Agency, 2.6.1 edition.

Gommenginger, C., Martin-Puig, C., Dinardo, S., Raney, K. R., Cipollini, P., Cotton, D., and Benveniste, J. (2010). Improved spatial resolution and range retrieval accuracy with sar altimeters over the ocean and the coastal zone: a numerical study. Ocean Surface Topography Science Team Meeting (OSTST), Lisbon International Fair, Lisbon, Portugal, 2010.

Gommenginger, C. and Srokosz, M. (2009). SAMOSA WP5.3 technical note. development & testing of SAR altimeter waveform theoretical retracker. Technical report, National Oceanography Centre, Southampton.

Stenseng, L. (2009). Samosa WP8 technical note. validation using airborne ASIRAS data. Technical report, DTU-Space.

Stenseng, L., Hvidegaard, S. M., Skourup, H., Forsberg, R., Andersen, C. J., Hanson, S., Cullen, R., and Helm, V. (2007). Airborne lidar and radar measurements in and around Greenland, CryoVEx 2006. Technical Report 9, Danish National Space Center.

A Abbreviations and acronyms

ASIRAS	Airborne SAR/Interferometric Radar Altimeter System
CryoVEx	CryoSat Validation Experiment
DTU-Space	National Space Institute, Technical University of Denmark
ESA	European Space Agency
HAM	High Altitude Mode
OCOG	Offset Center of Gravity
PRF	Pulse Repetition Frequency
SAR	Synthetic Aperture Radar
SARIn	SAR / Interferometry
SIRAL	SAR / Interferometric Altimeter
TN	Technical Note
WP	Work Package

B Response to review

Q1: The time gate spacing for CRYMPS and CryoSat is the inverse of the transmitted bandwidth; why such relation is not kept also for ASIRAS? .. the table 5 reports a gate spacing value that is not the inverse of the ASIRAS transmitted bandwidth.

A1: Cullen (2010) derives the range resolution in Equation 3.2-2 as:

$$\Delta R_{ham} = \frac{T_{uc} \cdot F_s \cdot c}{2 \cdot B \cdot N_{FFT\_ham}} \tag{4}$$

For ASIRAS in high altitude mode: $T_{uc} = 4\mu s$ (compressed pulse length), $F_s = 37.5MHz$ (instrument sampling frequency), $B = 1GHz$ (bandwisth), and $N_{FFT\_ham} = 256$ (range samples). Resulting in a range resolution of $\Delta R_{ham} = 0.08783m$ eqvivalent to a two-way time of 0.585e-9 s.

Q2: How much is reliable the value of 0.366 for ASIRAS PTR? Usually, this (0.37-0.4) is a pure theoretical value representing generally the minimum possible; given the limited nature of the on board hardware, usually it is quite hard to obtain in real conditions ... Has been performed any ASIRAS PTR calibration campaign to measure it? How has this value been derived?

A2: ASIRAS PTR is unknown, value from CryoSat-2 is adopted. Comment added in Section 4.1.

Q3: Please, report somewhere in the section 3 the exact time of acquisition (start time and stop time) and exact position of the location (start lat/lon stop lat/lon).

A3: Time and position added to Section 3

Q4: From the text, it emerges a pretty basic contradiction: at section 4.2 it is stated: "Pitch (i.e. along-track mispointing) is expected to strongly affect the positioning of the SAR waveforms (as well as the waveform shape)" but after it is noticed at section 4.3: "We see from these figures that the effect of mispointing will be much more dramatic for space borne systems (Figure 12) than for airborne systems (Figure 13), for which the waveforms are not expected to be strongly affected. Accordingly, the retracking of ASIRAS data will not account for along-track mispointing." : could you accommodate this contradiction stating in the conclusions that seemingly the actual shape of the model does not take in count properly the mispointing effects but a more enhanced version of the model to be provided in future will ??

A4: Section 4.3 rephrased to highlight the effect of the wide along-track beam on ASIRAS. The effect of mispointing in the SAMOSA1 model shows up only as a change in amplitude, not a change of waveform shape nor a shift in the position of the leading edge. Since we normalised waveforms prior to retracking, there is no effect by mispointing at present. Early results with the SAMOSA2 model suggest that the effect of mispoitning will be better accounted for in the enhanced model.

Q5: Did the retrieved height have been compensated by shift of the positioning due to the pitch mispointing? and in affirmative case how ?

A5: No effect of mispointing on leading edge position and no correction applied.

Q6: Could you show along with figure 14 (pitch along track in salient red points) also a similar graph but now plotting the roll angle in the same salient red points?

A6: Figure with roll and position of waveforms added to Section 4.4.

Q7: In figure 9 c) and d), we can notice how dramatically and quickly is changing the pitch and roll. It is presumably ascertainable that over such short over-flown fetch, the sea state must be constant; hence the only explanation for such dramatic waveform shape variability may be assigned only to the analogue mispointing variability: did you notice a correlation between the variability of roll and pitch with the variability of waveform shape width?

A7: Added comment and Figure 20 showing correlation between SWH and roll to Section 4.4.

Q8: Did you confront the obtained results for the sea surface elevation and SWH with some a priori known data over the same area: for example the Mean Sea Surface for the sea surface elevation and the SWH with SWH maps in the zone at the flight time? May you operate this in the scope of validation results activity?

A8: Results from the ECMWF wave model and DTU10 Mean Sea Surface added to Section 4.4 and 5.
ECMWF wave model (courtesy of Dr. Saleh Abdalla): Position of (78.1N, 3.4W) on 30 April 2006:

	06 UTC	12 UTC
Sig. Wave Height	1.83 m	1.46 m
Peak Period Tp	10.15 s	10.15 s
Mean Period T01	6.67 s	6.41 s
Mean Period T02	5.76 s	5.50 s
Mean Direction	220°	199°

Q9: Always in the scope of validation results activity, could you provide some statistics (mean, global standard deviation, relative standard deviation (standard deviation inside a 1 Hz subset)) for the surface elevation and SWH plots for OCOG and SAR retracker? Could you overlap the plots for surface elevation in order to visually confront the results coming from both methods?

A9: Figure 19 updated with running average on the SWH and surface elevation and comment added to Section 4.4.

Q10: As stated, the absence of the long trailing edge in ASIRAS data (unlike the model) can be explained by the short ASIRAS 3db beamwidth pattern in across-track direction; could you state in the conclusions that a more enhanced version of the model taking in count an asymmetric elliptical antenna pattern to be provided in future may correct this anomaly??

A10: The exact formulation and implementation of the enhanced model has not been fixed at this point.

DTU Space
National Space Institute
Technical University of Denmark

Juliane Maries Vej 30
DK-2100 København Ø

Tel +45 3532 5700
Fax +45 3536 2475

http://www.space.dtu.dk

ISBN: 978-87-92477-07-1